# Synthesis of Polymer-like Hydrogenated Amorphous Carbon by fs-pulsed Laser Induced Plasma Processing of Solid Hexane

Michal J. Wesolowski,* Brad Moores, Zoya Leonenko, Reza Karimi, Joseph H. Sanderson, Walter W. Duley

A new technique, that involves the plasma processing of frozen hydrocarbons by a pulsed laser generated graphitic plasma, is presented. Polymer-like hydrogenated amorphous carbon (a-C:H) thin films were created by allowing the plasma generated during the fs-pulsed laser ablation of a highly oriented pyrolytic graphite target in high vacuum, to impact on solid layers of *n*-hexane ($CH_3(CH_2)_4CH_3$) at 77 K. This technique results in the formation of thin films whose morphology and properties are shown to depend on the plasma processing time $t_p$. Polymer-like a-C:H with residual hexane incorporated into the carbon matrix and exhibiting a unique dendritic surface morphology was formed after short processing times. Following longer processing times, these dendritic structures are destroyed resulting in thin films having similar spectral properties to those of conventional a-C:H. The composition of the plasma was studied using time of flight mass spectrometer (TOF-MS) and the surface morphology of the synthesized thin films was examined by atomic force microscopy (AFM). A variety of analytic techniques including photoluminescence (PS), UV–Vis absorption, surface enhanced Raman (SERS), and Fourier transform infrared (FTIR) spectroscopy have been used to characterize the structure and composition of these materials.

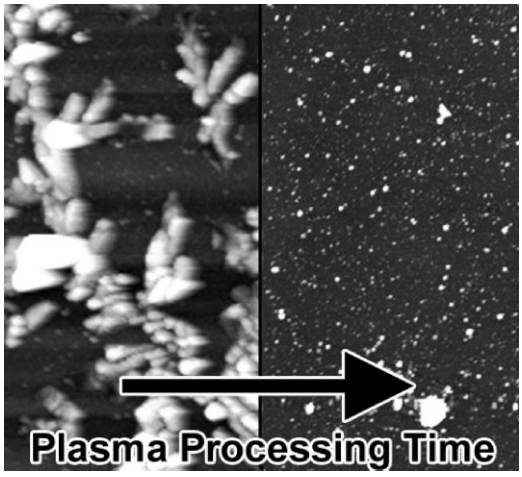


## 1. Introduction

Hydrogenated amorphous carbon (a-C:H) has a unique blend of optical, electronic, and mechanical properties. The overall composition and structure can range from graphite or polymer-like to diamond-like depending on the initial fabrication conditions and the hydrogen content. Owing to this versatility, a-C:H has numerous applications in a variety of industrial settings.[1] Pulsed laser deposition (PLD) has been shown to be an effective method for synthesizing a wide range of amorphous carbon (a-C). An advantage of PLD is that the properties of the deposited material can be tuned by selection of laser parameters, target material, and deposition environment.

In early work, Malshe et al.[2] produced a-C:H by the ns-PLD of graphite under a constant partial pressure of

M. J. Wesolowski, B. Moores, Prof. Z. Leonenko, R. Karimi, Prof. J. H. Sanderson, Prof. W. W. Duley
Department of Physics and Astronomy, University of Waterloo, 200 University Avenue West, Waterloo, Ontario N2L 3G1, Canada
E-mail: m2wesolo@uwaterloo.ca




DOI: 10.1002/ppap.201100206

hydrogen (0.45 Torr) using pulses from a ruby laser. The resulting amorphous thin films were smooth, chemically inert, weakly absorbing in the infrared and had an increased optical band gap when compared to non-hydrogenated PLD films. Several similar studies on the ns-PLD of a-C:H have shown that the properties of a-C:H films depend on substrate temperature, laser fluence, and gas pressure.[3–5] More recently Hu and Duley[6] have explored fs-PLD of graphite in a variety of hydrocarbon gases using a Ti:Sapphire laser system. Thin films deposited in the presence of hydrogen, acetylene, or ethylene were found to be partially composed of polycyclic aromatic hydrocarbons linked with polyyne chains. The shape and size of these molecular inclusions was found to be dependent on the type of gas present during the ablation process. These results differed significantly from those of similar a-C:H films synthesized by ns-PLD.

The ablation of target materials containing both carbon and hydrogen, such as carbon polymers or frozen hydrocarbons, has also been used to deposit a-C:H thin films by PLD.[7–10] Voevodin et al.[7] showed that a-C:H films, generated by ns-KrF laser irradiation of a polycarbonate target, undergo a graphitic to diamond-like structural transformation at laser fluences between $10^8$–$10^9$ W · cm$^{-2}$. Budai et al.[8] defined a volumetric intensity parameter $I_{vol}$, related to the power density in the target, to compare a-C:H formed by PLD of polymer targets using ns- and fs-pulsed laser systems and found that films produced at $I_{vol} \approx 10^{12}$–$10^{13}$ W · cm$^{-3}$ resembled the original polymer targets while those deposited at $I_{vol} \approx 10^{16}$ W · cm$^{-3}$ were amorphous. The composition of a-C:H from PLD of frozen hydrocarbon targets has been studied by the Hanabusa group. In their initial work, chemically inert, highly resistive a-C:H was fabricated by the ns-PLD of frozen acetylene.[9] Later, it was shown that the fs-PLD of frozen acetylene produced black conductive films, and the properties of deposited a-C:H could be changed by varying the composition of the frozen target.[10]

In this paper, we outline the results of a newly developed technique used for the synthesis of a-C:H thin films. This method involves the processing of frozen hydrocarbon layers by exposure to the carbon plasma generated by the ablation of graphite with fs laser pulses. In order to simplify the chemistry explored in this initial work we limit our discussion to deposits formed by carbon plasma processing of *n*-hexane ($CH_3(CH_2)_4CH_3$). The composition of the plasma was studied using time of flight mass spectrometer (TOF-MS) and the surface morphology of the synthesized thin films was examined by atomic force microscopy (AFM). A variety of spectroscopic techniques were employed to determine the thin film composition including photoluminescence (PS), UV–Vis absorption, surface enhanced Raman (SERS), and Fourier transform infrared (FTIR) spectroscopies.

## 2. Experimental Section

### 2.1. Deposition

Thin films were synthesized by the deposition of energetic carbon plasma, generated from the fs-pulsed laser ablation of graphite, onto pre-existing frozen hydrocarbon layers in vacuum. A schematic of this technique is shown in Figure 1 and from this point forward the plasma processing of any solid using this method will be referred to as pulsed laser induced plasma processing (PLIPP). In the present experiment, hexane (CHROMASOLV ≥97.0% from Sigma–Aldrich) was injected into a stainless steel vacuum chamber raising the base pressure from $5 \times 10^{-7}$ to $5 \times 10^{-4}$ Torr. This gas was then allowed to condense onto a cryogenically cooled substrate forming a polycrystalline alkane layer (Figure 1a). Optical grade fused quartz or potassium bromide (KBr) disks in thermal contact with a liquid nitrogen reservoir were used as substrates. The thickness of the frozen hexane was controlled by monitoring the time that the substrate was exposed to the gas. Once a layer was formed the excess gas was evacuated from the chamber. At this point a 300 μJ regeneratively amplified Ti:Sapphire tabletop laser with a 1 kHz repetition rate was used to generate 100 fs laser pulses with a central wavelength of 800 nm. The laser beam was focused onto a target within the vacuum chamber using a 0.16 m focusing lens which resulted in a peak focal intensity of $2 \times 10^{14}$ W · cm$^{-2}$. Inside the chamber a disk of highly oriented pyrolytic graphite (HOPG) served as the laser ablation target and was positioned parallel to the alkane covered substrate at a distance of 0.04 m (Figure 1b). The energetic carbon plasma, resulting from pulsed laser ablation, was then deposited on top of the frozen hexane layer

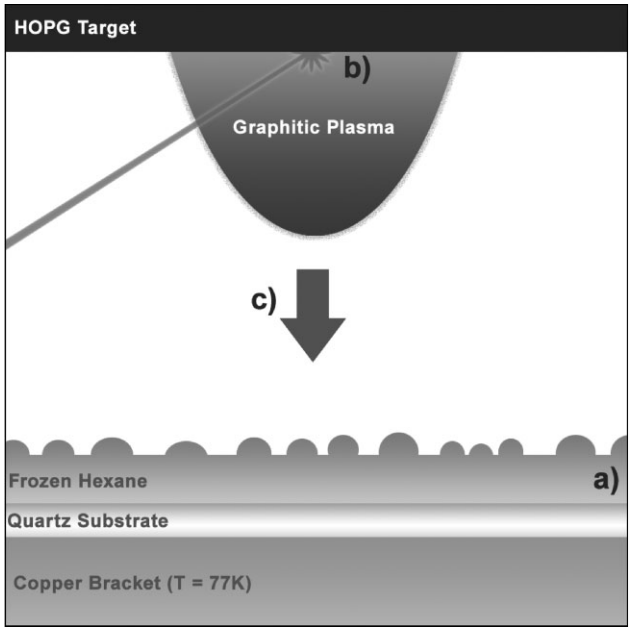


*Figure 1.* A schematic of the PLIPP process. (a) polycrystalline layers of hexane are initially deposited onto a substrate held at 77 K. After these frozen layers are deposited, (b) fs-laser pulses ablate an HOPG target forming a plasma. This plasma is then used (c) to process the frozen hexane layers, resulting in a residual hydrocarbon deposit.



DOI: 10.1002/ppap.201100206

over a set amount of processing time, $t_p$; either for five, ten or twenty minutes (Figure 1c). After deposition the samples were kept in vacuo until their temperature reached 293 K after which time they were exposed to atmosphere for analysis.

### 2.2. Characterization

The carbon plasma generated with the Ti:Sapphire laser system was characterized using a custom built TOF-MS with a micro-channel plate detector (MCP) at the end of 1 m long flight tube. The TOF for $H^+$ and $C^+$ ions ablated from the target were typically 1.4 and 4.25 μs, respectively. TOF spectra were recorded at delays of up to 100 μs with a mass resolution $\Delta m/m = 10^{-3}$. Thin film morphology was examined using AFM on a Nanowizard II AFM (JPK Instruments AG, Berlin, Germany) in intermittent air contact mode using Nanoworld NCH tips with 42 $Nm^{-1}$ spring constants. The optical properties of the films were determined using UV–Vis absorption and PS while the molecular bonding structure was studied through FTIR and SERS. UV–Vis and IR measurements were performed on Shimadzu UV-2501PC and FT-IR 8400S spectrophotometers respectively. Raman data was gathered on a Renishaw micro-Raman Spectrometer with an objective magnification of 50× and an excitation wavelength of 488 nm (0.5 mW). To facilitate surface enhancement, colloidal silver nanoparticles, with diameter less than 50 nm, were deposited onto the surface of film samples. Photoluminescence (PL) data were obtained using the same Renishaw system.

## 3. Results and Discussion

### 3.1. Atomic Force Microscopy (AFM)

Figure 2 shows representative surface morphology of thin films after PLIPP for 5 min (Figure 2a), 10 min (Figure 2b), and 20 min (Figure 2c). The surface of thin films remaining after 5 min exposure is densely covered with dendritic-type structures. The shape and size of these features was found to vary but they can be separated into two general categories, which we will refer to as either fern or island-like. Fern-like dendrites (arrow in Figure 2a) consist of a long central axis that can grow in excess of 50 μm in length, and 200 nm in height. Branching structures appear to originate from nucleation sites along the entire length of the central axis. Island-like dendrites are more compact than their fern-like counterparts with branches protruding from a central nucleation site rather than from an elongated stem (circle in Figure 2a). Individually, these structures cover a surface area $\leq 25\ \mu m^2$, and reach a maximum height of 200 nm. Fractal aggregates generated by diffusion limited aggregation (DLA) often have a very similar appearance to the dendritic structures seen in these films.[11] After 10 min of plasma processing these features become smaller, reaching a maximum height of 160 nm and length of 10 μm, and are more widely spaced on the film surface indicating structural damage is being caused by the plasma. By the 20 min mark all long range surface features have disappeared leaving only individual nanoparticles ranging in height from 2 to 60 nm or small nanoparticle clusters. These final films appear quite similar to a-C deposited by standard fs-pulsed laser ablation of graphite. Overall, the average thickness of all films generated using this method was found to decrease from ≈48 nm after 5 min to ≈32 nm after 20 min. This indicates that the surface structures are residual hydrocarbon deposits left over after processing of solid hexane by the plasma accompanying the ablation of graphite with fs-laser pulses.

### 3.2. Raman and UV–Vis Spectroscopy

The normalized micro-Raman spectra of a-C:H thin films resulting from the PLIPP at various $t_p$ are shown in Figure 3. It is clear that these films change significantly as $t_p$ increases. The spectrum of samples synthesized after 5 min of processing is rather featureless and is dominated by a strong photoluminescent (PL) background (Figure 3a).

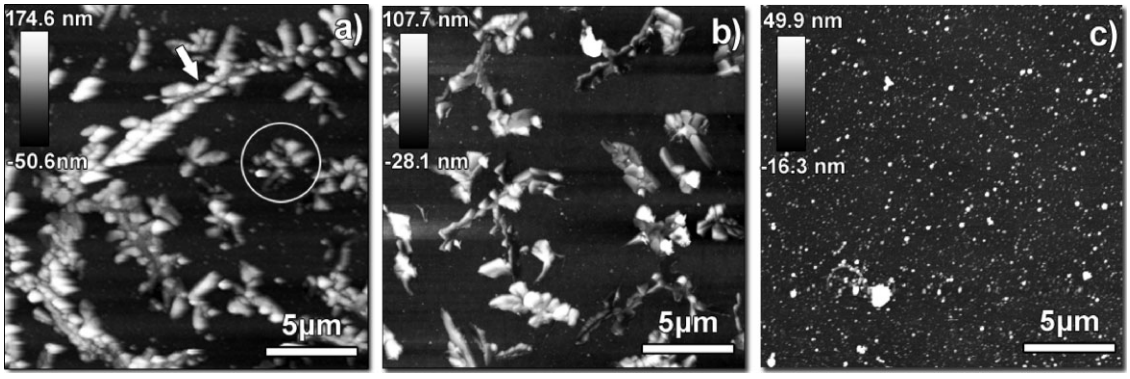


*Figure 2.* The evolution of surface structures on thin a-C:H films formed by allowing the plasma from the fs-laser ablation of graphite to impact on solid hexane after (a) 5 min, (b) 10 min and (c) 20 min of plasma exposure. The white arrow points to fern-like dendritic structures while an example of island-like structures is circled.

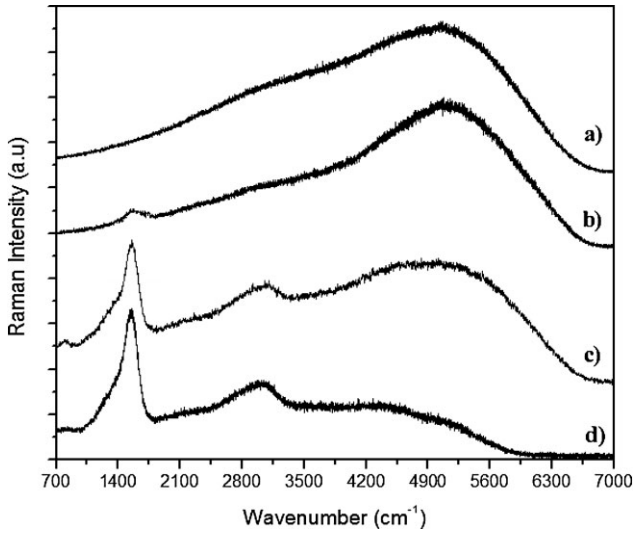


*Figure 3.* Room temperature normalized micro-Raman spectra of PLIPP thin films after (a) 5 min, (b, c) 10 min (high/low density of surface structure) and (d) 20 min of deposition onto solid hexane at 77 K. All spectra have been normalized and were obtained at an excitation wavelength of 488 nm.

Similar Raman spectra have been reported from polymer-like a-C:H, a soft, low density material that has a structure containing a significant number of H terminated $sp^3$ C bonds (60%) characterized by a high H content (40–50%), large optical band gap (2–4 eV), and low IR absorption.[12–14] It is well established that the PL intensity in a-C:H thin films relates directly to H concentration and complete obscurement of the prototypical *D* and *G* Raman modes occurs at H concentrations over 42 at.%.[15] This indicates a high level of H in films after short PLIPP. Two spectra are shown for films after 10 min of processing. In areas where there are still many surface features (Figure 3b) the large PL background continues to persist but the *D* peak, due to the breathing mode of sixfold $sp^2$ C rings and the *G* peak, resulting from the stretching of $sp^2$-bonded carbon, begin to appear at $\approx$1 500 $cm^{-1}$. This indicates that in these areas the H concentration has dropped <42 at.%. In regions with a lower density of surface features (Figure 3c) the PL background is further reduced and the Raman modes are enhanced. The spectrum of films after 20 min of processing (Figure 3d) is practically devoid of PL and resembles the spectrum typical of a-C:H with $\approx$20 at.% H.[14] The optical gap, $E_{04}$, which may be obtained directly from UV–Vis absorption data also correlates strongly to the hydrogen content in a-C:H.[16] We find that the optical gap decreases from 2.4 eV in films processed for 5 min to 1.6 eV in films processed for 20 min. This is an indication that the hydrogen decreases with processing time. Additional information about thin film composition can be gained by examining the evolution of the *D* and *G* mode Gaussian fitting parameters; as summarized in Table 1. While the energies of the *G* and *D* modes are relatively constant, there is a significant increase in the width of both modes with $t_p$ signaling an increase in internal stress within the a-C:H matrix. This can be attributed to a decrease in hydrogen content and/or an increase in bond disorder.[15,17] Amorphous carbon is typically viewed as a collection of independent $sp^2$ clusters bonded to an $sp^3$ carbon matrix. The size of these clusters may be determined by taking the ratio of the intensities of the *D* and *G* modes, $I_D/I_G = cL_a$ where *c* is a fitting parameter. The value of this ratio increases with the number of rings (size) forming the clusters and therefore indicates the degree of graphitization of the material.[18,19] In our films this value scales with $t_p$ and changes from $I_D/I_G = 0.21$ when $t_p = 10$ min to $I_D/I_G = 0.51$ after $t_p = 20$ min suggesting that plasma processing causes graphitization of the underlying hexane layer.

### 3.3. Surface Enhanced Raman Spectroscopy (SERS)

Information about the specific molecular content of polymer-like a-C:H cannot normally be obtained with visible Raman spectroscopy but the SERS effect enhances the intensity of vibrational modes in many molecular species allowing for their identification using visible wavelengths. Figure 4 shows SERS spectra of films after various $t_p$ as well as the Raman spectrum of liquid hexane over the 250–2 250 $cm^{-1}$ range. In this region the spectral profile of hexane (Figure 4a) results mainly from methyl ($-CH_3$) and methylene ($-CH_2-$) group deformations (1 300–1 480 $cm^{-1}$), C–C stretching (600–1 300 $cm^{-1}$) vibrations and longitudinal acoustic modes (250–400 $cm^{-1}$).[29,21] The most prominent feature occurs at 1 448 $cm^{-1}$ and results from the symmetric scissor type

*Table 1.* Fitting parameters of the Raman *D* and *G* modes and optical band-gap energy of thin films formed after various processing times.

| Thin film | $G_{pos}$ [$cm^{-1}$] | $G_{FWHM}$ [$cm^{-1}$] | $D_{pos}$ [$cm^{-1}$] | $D_{FWHM}$ [$cm^{-1}$] | $I_D/I_G$ | $E_{04}$ [eV] |
|---|---|---|---|---|---|---|
| 5 min (Figure 2a) | n/a | n/a | n/a | n/a | n/a | 2.4 |
| 10 min (Figure 2b) | 1 556 ± 1 | 102 ± 3 | 1 389 ± 2 | 201 ± 3 | 0.21 | 1.9 |
| 10 min (Figure 2c) | 1 556 ± 1 | 126 ± 1 | 1 391 ± 3 | 335 ± 10 | 0.46 | 1.9 |
| 20 min (Figure 2d) | 1 554 ± 1 | 136 ± 1 | 1 396 ± 1 | 309 ± 2 | 0.51 | 1.6 |



DOI: 10.1002/ppap.201100206

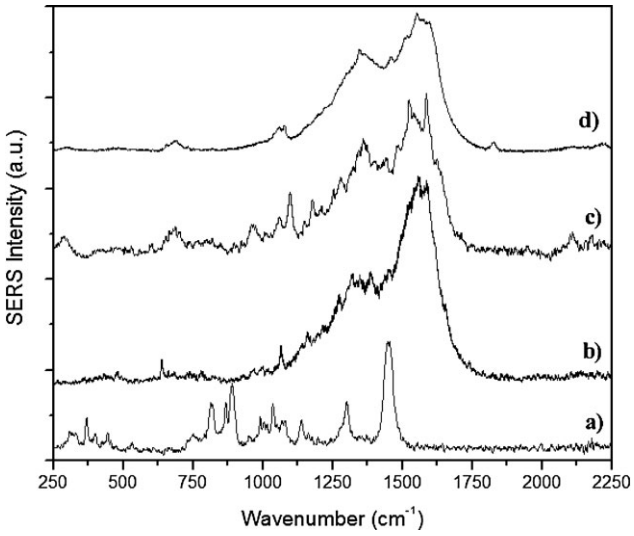


*Figure 4.* The normalized Raman spectrum of liquid hexane (a) and the surface enhanced Raman spectra of thin films processed for (b) 5 min, (c) 10 min and (d) 20 min, excited by the 488 nm $Ar^+$ laser line. Samples were at room temperature.

deformation of methylene. This vibration occurs in numerous hydrocarbon molecules and its spectral position can vary from 1 440 to 1 480 $cm^{-1}$. In the SERS data from thin film samples, discrete spectral features not present in conventional Raman appear due to selective plasmonic enhancement and the most prominent vibrational modes with their probable assignments are summarized in Table 2. The overall spectral envelope of films processed for 5 min (Figure 4b) resembles that of a-C:H obtained by conventional Raman but the PL background has been suppressed and a large number of small sharp peaks appear. In the *G* mode region (1 500–1 640 $cm^{-1}$) there are a series of peaks that can be attributed to different $sp^2$ bonded species, with ring vibrations resulting in lower frequency peaks and contributions from conjugated C=C chains giving peaks >1 600 $cm^{-1}$.[18] Some care must be taken when considering the origin of peaks in the *D* region (1 300–1 400 $cm^{-1}$) as visible Raman C–H modes do not normally contribute to the *D* mode intensity as they are not optically active; however, this is not the case in SERS. Therefore, peaks occurring in this region may arise not only from sixfold ring breathing vibrations but also from the deformation modes of methyl, ethyl ($-C_2H_5$), butyl ($-C_4H_9$) and propyl ($-C_3H_7$) groups.[21] The appearance of skeletal modes associated with alkyl groups (1 100–1 300 $cm^{-1}$) helps to confirm that this is in fact the case. Given that hexane is a fully $sp^3$ bonded hydrocarbon containing two methyl groups it is not surprising that similar group vibrations are also present in thin films synthesized through PLIPP. It is also significant that a number of peaks in lightly processed films are almost exactly coincident with hexane vibrational modes and include the symmetric methylene scissor vibration occurring at 1 449 $cm^{-1}$.[19,21] Combined with the presence of additional methylene modes such as the wagging vibration at 1 301 $cm^{-1}$, this suggests that hexane molecules are being incorporated into the a-C:H matrix in a relatively intact state. After further processing it is expected that these molecules may be dissociated which should result in additional methyl and methylene vibrational modes since their spectral position is somewhat dependent on chain length. This does appear to be the case in the spectrum of films that have been processed for 10 min (Figure 4c). In addition to the peaks in the *D*, *G* and C–C stretching regions

*Table 2.* Energies of primary SERS vibrational spectral features after various plasma processing times.

| Vibrational mode | 5 min[a] peak position [$cm^{-1}$] | 10 min[b] peak position [$cm^{-1}$] | 20 min[c] peak position [$cm^{-1}$] | Reference |
|---|---|---|---|---|
| Hexane | 1 449, 1 301, 1 287, 1 196, 1 178, 1 162, 1 079, 1 068, 1 049, 887, 790 | 1 302, 1 286, 1 177, 1 137 | 1 301, 1 287, 1 197, 1 163 | Figure 4a, [20,21] |
| sp C | | 2 176, 2 155, 2 109, 2 100 | 2 219, 2 208, 1 826 | [22,23] |
| $sp^2$ *G* | 1 640, 1 612, 1 586, 1 558, 1 522 | 1 623, 1 601, 1 585, 1 546, 1 522 | 1 616, 1 549, 1 522 | [18] |
| $(-CH_3)_n$ def. | 1 422, 1 385 | 1 483, 1 452, 1 445, 1 440, 1 400, 1 371 | 1 458, 1 430 | [20,21] |
| $sp^2$ *D* | 1 347 | 1 360 | 1 346, 1 365 | [18] |
| C–C str. | 1 271, 1 168, 1 064 | 1 252, 1 211, 1 190, 1 148, 1 100, 1 096 | 1 246, 1 226, 1 076, 1 057 | [20,21] |

[a]Figure 4b; [b]Figure 4c; [c]Figure 4d.

there are now several additional peaks in the 1 400–1 500 $cm^{-1}$ range which result from different configurations of the asymmetric methyl and methylene scissor deformation vibrations. An additional feature that is of interest in the spectra of thin films processed for 10 min is the appearance of modes in the 1 800–2 200 $cm^{-1}$ region associated with the vibrations of straight chain sp carbon polyynes ($C_{2n}H_2$) or cumulenes ($C_nH_4$).[22,23] These modes are consistent with the formation of polyynes and polycumulenes in a-C:H at low hydrogen content.[24] The spectrum of films processed for 20 min (Figure 4d) resembles that of a more traditional a-C:H with low hydrogen content and contains fewer peaks in the methyl and methylene spectral range. These are likely to result from $sp^2$ bonded carbons given the increase in the *D* mode intensity seen in the visible Raman spectra of these films (Figure 4d).

### 3.4. Fourier Transform Infrared Absorption

Figure 5 shows IR spectra of as-produced a-C:H thin films in the 2 800–3 100 $cm^{-1}$ range. This spectral region can be separated into two sub-regions; the stretching modes of $sp^3$ CH groups near 2 850–2 955 $cm^{-1}$ and that of $sp^2$ bonded CH at 2 975–3 085 $cm^{-1}$.[25,26] The most prominent band in all spectra occurs near 2 920 $cm^{-1}$ and results from the anti-symmetric methylene stretching mode. It is paired with the weaker symmetric mode at 2 853 $cm^{-1}$. The symmetric and anti-symmetric stretching modes of the methyl group at 2 883 and 2 958 $cm^{-1}$, respectively, are also present in the spectra of films processed for 5 and 10 min. These modes are missing or have reduced intensity in films after with $t_p = 20$ min. This trend follows that found in the SERS data and the presence of these modes helps to confirm the previous peak assignments. A variety of other modes such as those from olefinic $CH_2$ at 2 975 and 3 078 $cm^{-1}$ are also present in these samples but are of much lower intensity. Olefinic CH, with modes in the 2 986–3 002 $cm^{-1}$ range and aromatic CH arising from 3 032–3 059 $cm^{-1}$ are also present in IR spectra of all samples.

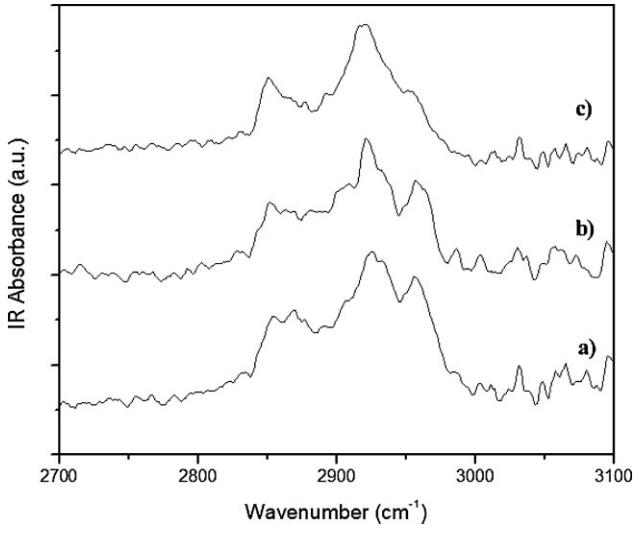


*Figure 5.* The IR absorption spectra at 300 K of thin films after (a) 5 min, (b) 10 min and (c) 20 min of plasma processing.

An additional issue that should be mentioned when discussing the composition of any plasma deposited thin film is the possibility of oxidation and aging due to exposure to atmospheric oxygen and water. It is well established that plasma polymerized thin films contain high concentrations of free radicals which readily react with oxygen to form chemically bonded species within a given film.[27–29] The present samples show no evidence of oxidation within the first 24 h after deposition. Typically, features associated with C=O occur in the 1 640–1 900 $cm^{-1}$ IR spectral region,[30] but no such features were apparent in our data. This is not wholly unexpected since it has been recently shown that a-C:H thin films deposited using different methods, do not react strongly with oxygen.[30,31] This of course does not preclude the presence of a small percentage of oxygen (<3%) within the present films, and more sensitive techniques could be employed to determine the role of oxygen. It would be interesting to study this effect, as well as the long-term temporal stability of films formed by PLIPP.

## 4. Discussion

Plasma deposited a-C:H thin films produced using traditional synthesis techniques, such as plasma enhanced chemical vapor deposition (PECVD) or PLD, lack long range order and have a relatively simple molecular composition due to the inherently disordered mechanism by which they are formed. When carbon and hydrocarbon plasma species impact a surface they may undergo a variety of physical and chemical interactions including physisorption, H abstraction, dissociation, addition, and ion subplantation. All of these processes are thought to contribute to the growth of a-C:H thin films; however, under most deposition conditions subplantation is dominant.[32–34] In many cases, these films have a very simple surface morphology. Some have atomic smoothness while others are rough and are assembled from individual nanoparticles. The overall structure has been found to be a strong function of ion energy and substrate temperature.[33] The surface structure of thin films formed by PLIPP of solid hexane after short exposure times are remarkably different from those of standard a-C:H thin films. For example, the appearance of long range dendritic ordering in carbon films has not been reported previously and likely results from the interaction between the laser produced plasma and the surface of solid hexane.



DOI: 10.1002/ppap.201100206

*Table 3.* Selection of the most prominent low mass ions in carbon plasma from graphite.

| Ion | *m/q* [C mass/charge] | Time [$1 \times 10^{-6}$ s] |
|---|---|---|
| $C^{4+}$ | 0.065 | 2.16 |
| $C^{3+}$ | 0.114 | 2.48 |
| $C^{2+}$ | 0.257 | 3.04 |
| $C_2^{2+}$ | 0.988 | 4.23 |
| $C^{+}$ | 1.00 | 4.24 |
| $CH^{+}$ | 1.08 | 4.40 |
| $C_2^{+}$ | 1.98 | 5.96 |
| $C_2H^{+}$ | 2.08 | 6.12 |
| $C_3^{+}$ | 3.01 | 7.36 |
| $C_3H^{+}$ | 3.08 | 7.44 |

The plasma produced by fs-pulsed ablation of graphite consists primarily of electrons and small positively charged carbons and hydrocarbons (see Table 3). When this plasma impacts the polycrystalline surface of solid hexane it is expected to result in dehydrogenation and the production of a variety of volatile species including $CH_4$. Additionally, dehydrogenation and photo-dissociation can be initiated by processing as a result of UV radiation emitted by the plasma, although this effect is considered to be small compared to that of ion bombardment.[35] While there have been no direct studies on the effects of carbon ion bombardment on frozen hexane, a number of authors have examined the effects of $He^{+}$ bombardment on frozen butane and benzene. In both cases a-C:H residues were formed with progressive carbonization due to increasing ion dosage.[36,37] In the present configuration, sub-surface carbon ion implantation and carbon insertion reactions will build larger carbon networks. It appears that hexane molecules are incorporated at this early stage and are retained in the solid after warming to 300 K. Continued exposure to the plasma eventually results in the formation of an amorphous carbon film. This sequence is confirmed through the spectroscopic analysis of the PLIPP films preformed ex situ. After brief plasma exposure, the composition of these films is similar to that of polymer-like amorphous carbon with a significant hexane component. Upon additional plasma processing, SERS and FTIR data indicate that the hexane molecules within the carbon matrix begin to dissociate, likely due to further reaction with C atoms. This also leads to erosion of the dendritic structures (Figure 2b) and a decrease in H content through abstraction as evidenced by a decreasing PL background and optical band gap. At long $t_p$, all distinct long range surface features have been destroyed and the remaining deposits have a surface structure similar to that of traditionally synthesized a-C:H.

## 5. Conclusion

A new method for the formation of thin a-C:H films is described in which a solid hexane layer at 77 K is processed through exposure to the plasma generated during the fs laser ablation of graphite. The resulting films have a unique dendritic surface morphology and are polymer-like with strong room temperature PL. Upon further plasma processing these surface structures are gradually destroyed resulting in a nanoparticle assembled amorphous carbon film. Dendritic films are found to retain parent hexane molecules which become incorporated in the solid. This suggests that it may be possible to use the PLIPP technique to generate carbonaceous materials with tailored physical and chemical properties based on networks of $sp^2$ rings separated by specific distances defined by the length of individual alkane chains. Amorphous carbon thin films have been suggested for use as molecular sieves[38,39] and tailored carbon networks generated by PLIPP could potentially be implemented in this type of application.

Acknowledgements: This work was financial supported by the Natural Sciences and Engineering Research Council of Canada (NSERC), the Canada Foundation for Innovation (CFI) and the Ontario Research Fund (ORF).

Received: November 25, 2011; Revised: January 24, 2012; Accepted: January 26, 2012; DOI: 10.1002/ppap.201100206

Keywords: femtosecond-pulsed laser induced plasma processing; hydrocarbon; nanostructures; polymer-like amorphous carbon; surface enhanced Raman spectroscopy

[1] A. Grill, *Diam. Relat. Mater.* **1999**, *8*, 428.
[2] A. P. Malshe, S. M. Kanetkar, S. B. Ogale, S. T. Kshirsagar, *J. Appl. Phys.* **1990**, *68*, 5648.
[3] D. L. Pappas, K. L. Saenger, J. Bruley, W. Krakow, J. J. Cuomo, T. Gu, R. W. Collins, *J. Appl. Phys.* **1992**, *71*, 5675.
[4] H. C. Ong, R. P. H. Chang, *Phys. Rev. B* **1997**, *55*, 13213.
[5] J. Budai, Z. Tóth, A. Juhász, G. Szakács, E. Szilágyi, M. Veres, M. Koós, *J. Appl. Phys.* **2006**, *100*, 043501.
[6] A. Hu, W. W. Duley, *Chem. Phys. Lett.* **2008**, *450*, 375.
[7] A. A. Voevodin, S. J. P. Laube, S. D. Walck, J. S. Solomon, M. S. Donley, J. S. Zabinski, *J. Appl. Phys.* **1995**, *78*, 4123.
[8] J. Budai, M. Bereznai, G. Szakács, E. Szilágyi, Z. Tóth, *Appl. Surf. Sci.* **2007**, *253*, 8235.
[9] M. Hanabusa, K. Tsujihara, *J. Appl. Phys.* **1995**, *78*, 4267.
[10] M. Okoshi, S. Higuchi, M. Hanabusa, *J. Appl. Phys.* **1999**, *86*, 1768.
[11] T. A. Witten, L. M. Sander, *Phys. Rev. B* **1983**, *27*, 5686.
[12] D. L. Baptista, F. C. Zawislak, *Diam. Relat. Mater.* **2004**, *13*, 1791.

[13] B. Marchon, J. Gui, K. Grannen, G. C. Rauch, J. W. Ager, III, S. R. P. Silva, J. Robertson, *IEEE Trans. Magn.* **1997**, *33*, 3148.
[14] J. G. Buijnsters, R. Gago, I. Jiménez, M. Camero, F. Agulló-Rueda, C. Gómez-Aleixandre, *J. Appl. Phys.* **2009**, *105*, 093510.
[15] J. Schwan, S. Ulrich, V. Batori, H. Ehrhardt, S. R. P. Silva, *J. Appl. Phys.* **1996**, *80*, 440.
[16] A. Golanski, F. Piazza, J. Werckmann, G. Relihan, S. Schulze, *J. Appl. Phys.* **2002**, *92*, 3662.
[17] J. Filik, P. W. May, S. R. J. Pearce, R. K. Wild, K. R. Hallam, *Diam. Relat. Mater.* **2003**, *12*, 974.
[18] A. C. Ferrari, J. Robertson, *Phys. Rev. B* **2000**, *61*, 14095.
[19] F. F. Cleveland, P. Porcelli, *J. Chem. Phys.* **1950**, *18*, 1459.
[20] V. S. Gorelik, A. V. Chervyakov, L. V. Kol'tsova, S. S. Veryaskin, *J. Russ. Laser Res.* **2000**, *21*, 323.
[21] G. Socrates, *Infrared and Raman Characteristic Group Frequencies: Tables and Charts*, John Wiley & Sons, Chichester, West Sussex, England **2001**.
[22] H. Tabata, M. Fujii, S. Hayashi, T. Doi, T. Wakabayashi, *Carbon* **2006**, *44*, 3168.
[23] L. Ravagnan, P. Piseri, M. Bruzzi, S. Miglio, G. Bongiorno, A. Baserga, C. S. Casari, A. Li Bassi, C. Lenardi, Y. Yamaguchi, T. Wakabayashi, C. E. Bottani, P. Milani, *Phys. Rev. Lett.* **2007**, *98*, 216103.
[24] A. Hu, Q.-B. Lu, W. W. Duley, M. Rybachuk, *J. Chem. Phys.* **2007**, *126*, 154705.
[25] M. Veres, M. Koós, I. Pócsik, *Diam. Relat. Mater.* **2002**, *11*, 1110.
[26] J. Ristein, R. T. Stief, L. Ley, W. Beyer, *J. Appl. Phys.* **1998**, *84*, 3836.
[27] I. Retzko, J. F. Friedrich, A. Lippitz, W. E. S. Unger, *J. Electron Spectrosc. Relat. Phenom.* **2001**, *121*, 111.
[28] S. Schiller, J. Hu, A. T. A. Jenkins, R. B. Timmons, F. S. Sanchez-Estrada, W. Knoll, R. Förch, *Chem. Mater.* **2002**, *14*, 235.
[29] F. Truica-Marasescu, M. R. Wertheimer, *Plasma Process. Polym.* **2008**, *5*, 44.
[30] A. Ogino, M. Nagatsu, *Thin Solid Films* **2007**, *515*, 3597.
[31] Y. Yun, X. Ma, J. Gui, E. Broitman, A. J. Gellman, *Langmuir* **2007**, *23*, 5485.
[32] W. Möller, *Appl. Phys. A* **1993**, *56*, 527.
[33] Y. Lifshitz, G. D. Lempert, E. Grossman, *Phys. Rev. Lett.* **1994**, *72*, 2753.
[34] W. Jacob, *Thin Solid Films* **1998**, *326*, 1.
[35] S. M. Wu, J. J. Lin, Y. T. Lee, X. Yang, *J. Phys. Chem. A* **2000**, *104*, 7189.
[36] G. Compagnini, R. Reitano, G. Foti, G. Baratta, G. Strazzulla, *Radiat. Eff. Defect. S.* **1991**, *117*, 299.
[37] G. Strazzulla, G. A. Baratta, *Astron. Astrophys.* **1992**, *266*, 434.
[38] Y. Yin, R. E. Collins, *Carbon*, **1993**, *31*, 1333.
[39] L. Valentini, M. C. Bellachioma, L. Lozzi, S. Santucci, J. M. Kenny, *J. Vac. Sci. Technol., A* **2002**, *20*, 1647.



DOI: 10.1002/ppap.201100206